Fabricating Arrays of Vanadium Dioxide Nanodisks by Focused Ion-Beam Lithography and Pulsed Laser Deposition

R. F. Haglund, Jr.[*a], R. Lopez[a], J. Y. Suh[a], L. C. Feldman[a,b], T. E. Haynes[b] and L. A. Boatner[b]

[a]Department of Physics and Astronomy and Institute for Nanoscale Science and Engineering
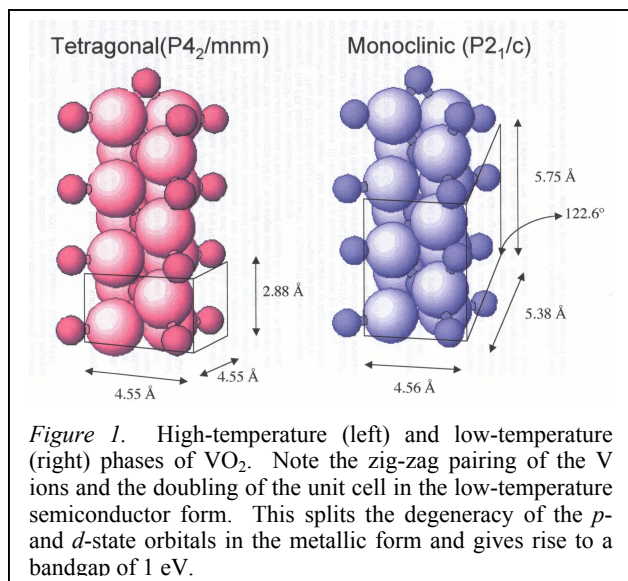Vanderbilt University, Nashville TN 37235-1807 U.S.A.
[b]Condensed-Matter Sciences Division, Oak Ridge National Laboratory, Oak Ridge TN 37831

ABSTRACT

Vanadium dioxide undergoes a structural (monoclinic to tetragonal) insulator-to-metal transition at 70°C, accompanied by large changes in electrical and optical properties. By combining focused ion-beam lithography and pulsed laser deposition, patterned nanoscale arrays of vanadium dioxide nanoparticles are created that can be used for studies of linear and nonlinear optical physics, as well as demonstrating the potential for a variety of applications.

1. INTRODUCTION AND MOTIVATION

The search for "smart materials" that alter their physical or chemical state in response to an external stimulus is an important and continuing topic in materials science. It has been known since the late 1950s that vanadium dioxide (VO_2) was such a material; it undergoes a semiconductor-to-metal transition at a temperature of about 70°C, and exhibits a hysteretic return to the semiconducting state when cooled.[2] This reversible change is accompanied by a slight alteration in structure from the monoclinic crystalline form of the semiconductor to the tetragonal metallic form. This tiny change in structure, in turn, leads to a hundred-thousand-fold increase in electrical conductivity! Similar striking changes are apparent in the optical transmission of thin films of vanadium dioxide. This has led to consideration of VO_2 as a "smart material" in applications such as optical limiting, non-volatile memory, thermochromic windows [3], and ultrafast optical switches.[4, 5] The last applications category is particularly interesting because the transition is known to occur at time scales significantly shorter than 1 ps.

Figure 1. High-temperature (left) and low-temperature (right) phases of VO_2. Note the zig-zag pairing of the V ions and the doubling of the unit cell in the low-temperature semiconductor form. This splits the degeneracy of the *p*- and *d*-state orbitals in the metallic form and gives rise to a bandgap of 1 eV.

However, nothing was known about the nanocrystalline behavior of VO_2 until a breakthrough in ion-beam synthesis enabled us to create thin layers of size-controlled VO_2 nanocrystals in a fused silica matrix with a dramatically increased hysteresis between heating and cooling cycles.[6] When the thermodynamics of the phase transition was mapped as a function of nanocrystal size by measuring the change in optical properties,[7] it exhibited a definite size dependence hinting at a novel nucleation mechanism. Nevertheless, it was clear that dynamical studies would require much greater uniformity in size and size distribution than the ion implantation synthesis was capable of delivering.

Recently, in order to have better control over morphology, size and size distribution, we have developed a technique for fabricating arrays of stoichiometric VO_2 nanodisks that combines focused ion-beam lithography with pulsed laser deposition and appropriate annealing. In the following paper, this method is briefly described, and some initial results of optical characterization of the nanoparticle arrays are presented, along with possible future directions.

---

[*] *Richard.Haglund@vanderbilt.edu*, phone 1-615-322-7964, fax 1-615-343-7263, *www.physics.vanderbilt.edu*

2. MECHANISM OF THE PHASE TRANSITION

Vanadium dioxide undergoes a metal-insulator transition at 70°C due to a structural phase change from a monoclinic semiconducting structure to a tetragonal metallic structure. This lattice rearrangement is exceedingly modest in terms of overall dimensions, but the structu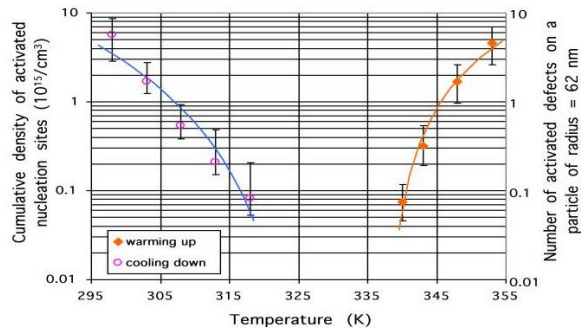ral change has striking effects on the properties of the VO_2. The lifting of the degeneracy in the V^+ ion states by the pairing of neighboring ions tilts the oxygen octahedral in the crystal structure, and opens up a band gap of approximately 1 eV. The phase transition is apparently initiated from still unidentified special sites in the nanoparticles, from which the structural change propagates through the entire nanocrystal. By measuring the transitions between the metallic and semiconducting phases of the VO_2 nanocrystals during heating and cooling cycles, it was demonstrate that both size and the number of special sites in the nanocrystals affect this transition. Figure 2 shows the classic form of the first-order phase transition measured for VO_2 nanoparticles embedded in a fused silica matrix, and shows at what temperature a given size nanocrystal will change from a semiconductor to a metal or the reverse, depending on whether it is in the heating or cooling cycle. For example, during the heating cycle, a spheroidal nanocrystal of around 60 nm diameter will have one such special site on average, and will change from the semiconducting to the metallic phase at 345 K.

Figure 2. Number density of activated defects in a VO_2 nanoparticle as a function of temperature, showing the effects of nanoparticle size on the transition temperature in the cooling (blue) and heating (orange) metal-insulator transitions during which the structure changes from the low-temperature monoclinic form to the high-temperature tetragonal structure.

Although the mechanism of structural phase transitions has been settled for many of the transition-metal oxides — such as V_2O_3 and TiO_2 — the mechanism question has remained controversial for VO_2. The unit cell of the semiconducting phase is twice the size of the unit cell for the metallic phase, a hallmark of the Peierls-type lattice instability and one of the reasons for the continuing interest in this mechanism. There have also been arguments that the mechanism had to involve interatomic electron-electron correlations analogous to the Mott-Hubbard transition. The experimental evidence is ambiguous. For example, early studies of Raman scattering in VO_2 films showed a clear change in the Raman signature above and below the transition temperature.[8] More recent studies using Raman microscopy, on the other hand, show no effect and seem to hint that the origin of the transition is purely electronic.[9] At this point, the driving mechanism of the phase transition must be considered to be highly uncertain. Indeed, it is possible that the mechanism is a combination of both electronic and lattice contributions.[10] It is this uncertainty that drives, from the standpoint of phase-transition physics, the need for precise control of nanocrystal size and morphology in studies of vanadium dioxide at nanometer length scales.

Hubbard Mechanism (Electronic)		Peierls Mechanism (Lattice Instability)	
Property	Prediction	Period doubling of unit cell	Prediction
Magnetic properties	Yes	Pairing of metal atoms (zig-zag chain)	Yes
Narrowing of d-bands	Yes	Phonon softening (*e.g.*, in Raman spectra)	Perhaps
Sharp drop in conductivity at T_c	Yes	Large lattice latent transition heat	Yes
	Contradiction		Contradiction
Structural change	No	Fermi surface nesting not in c-axis	No
Phonon softening at T_c	No	Bandgap of order ~1 eV	No
Possible existence of charge-density wave	No	Change in conductivity of 10^4	Only 10^2
Predicts $dT_c/dP>0$ in bulk material	No	Predicts $dT_c/dP>0$ in bulk material	No
		$dE_{gap}/dP<0$ for bulk material	No

THE CHALLENGE OF STOICHIOMETRIC VO_2 NANOFABRICATION

The apparent sensitivity of the phase transition to both electronic and lattice interactions makes the issue of stoichiometry a significant one. Vanadium dioxide has been a particular challenge for materials synthesis because of the large number of vanadium oxides with similar stoichiometries that do not undergo the semiconductor-to-metal transition at the same temperature, if at all. As shown in the diagram below (figure 2), a plot of the stoichiomery as a function of temperature (left axis), there are many different oxides with stoichiometries similar to that of VO_2, and most of them have transition temperatures that are quite different transition temperatures; in one case, there is no phase transition at all!

This means that the synthesis process requires significant care as well as detailed verification of the composition of the nanoparticles.

A number of different techniques have been used to synthesize VO_2 in the form of single crystals and thin films. These include sol-gel [11-13], sputtering [14], ion-beam assisted deposition, RF plasma deposition, chemical vapor deposition and fabrication in powders of varying sizes and stoichiometries [15]. None of these techniques produce materials that are suitable for optical studies of the size dependence of the phase transition in VO_2. This is because electrical methods that work for thin films are extremely tricky to apply to nanocrystalline samples. The sol-gel samples already have problems in this regard because the samples are highly scattering. The powders, moreover, show a wide variation in nanocrystal size, thus rendering these samples essentially unusable for investigations of the mechanism of the structural phase transition.

The first successful attempts to fabricate nanocrystalline VO_2 of a suitable quality for optical investigations were reported by Boatner *et al.* using ion implantation.[16] These

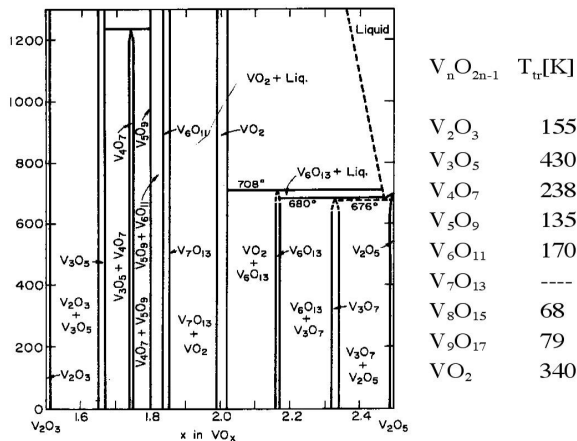| V_nO_{2n-1}	T_{tr}[K]
V_2O_3	155
V_3O_5	430
V_4O_7	238
V_5O_9	135
V_6O_{11}	170
V_7O_{13}	----
V_8O_{15}	68
V_9O_{17}	79
VO_2	340

Figure 3. Phase stability diagram for the vanadium oxides, showing regions of phase stability (with temperature) as a function of oxygen stoichiometry x.

were then followed by a series of breakthroughs in synthesizing and characterizing VO_2 nanoparticles generated by implantation of stoichiometric doses of vanadium and oxygen into fused silica substrates.[17] The energies of the ions were chosen such that the stoichiometry was essentially perfect in a thin (~100 nm) subsurface layer in the silica. Upon annealing to temperatures near 1000˚C in an Ar atmosphere, a thin layer of nanorods was formed, with the size of the nanorod depending on the time of annealing. During these experiments, it was learned that the only effective ways to verify the stoichiometry of a sample are to measure directly, for example by ion backscattering measurements.

3. APPARATUS: FOCUSED-ION BEAM AND PULSED LASER DEPOSITION SYSTEM

The need for substantial, differentiated control over the lithography, deposition and crystallization steps required to produce arrays seemed, from the first, to obviate the possibility of synthesizing stoichiometric VO_2 nanocrystalline materials in a single-step process. Thus a combination of lithography, deposition and post-deposition annealing was employed.

The arrays of VO_2 nanodisks fabricated in these experiments were patterned in an FEI/Philips FIB200 focused ion beam (FIB) writer, based on a a liquid Ga^+ ion source operating at 30 kV. The software interface of the FIB allows the user to input arbitrary lithographic patterns and to control ion-beam current on a pixel-by-pixel basis A solution of PMMA (standard molecular weight of 950 K) in anisole (1.7% by weight) was spun onto a glass substrate covered with a thin layer of indium-tin oxide (ITO) in two consecutive stages (first at 500 rpm for 5 seconds, then at 4000 rpm for 45 s) and baked on a hot plate at 180 ºC for 3 minute to obtain a uniform 50 nm layer. The thickness of the PMMA layer is chosen to match the projected range of the Ga^+ ions at 30 keV. The Ga^+ beam is focused to a nominal beam diameter of 8 nm to create the pattern of single pixel dot arrays on the PMMA; typical beam current is 1 pA, and typical dwell time per dot is 80 μs. The exposed PMMA was developed in a 1:3 methyl isobutyl ketone and isopropyl alcohol mixture to reveal the underlying surface.

The developed samples were coated by an $VO_{1.7}$ layer of the desired thickness (typically 20 nm) by pulsed laser deposition from a vanadium metal sputtering target purchased commercially in an oxygen ambient at 5 mTorr pressure. The laser deposition chamber was also a commercial unit (Epion PLD3000). Laser ablation of the target was accomplished
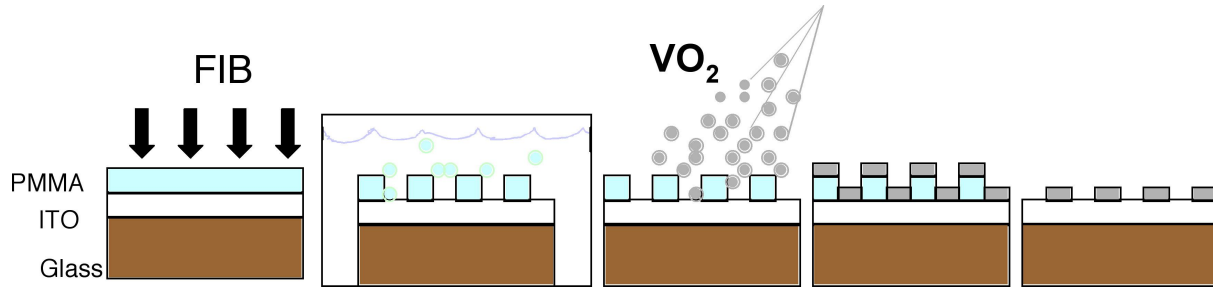
Figure 4. Steps in focused ion-beam lithographic fabrication of VO_2 nanoparticle arrays. From left: (1) The substrate is a sandwich of ITO on glass; the PMMA is spun on, and the FIB then irradiates the PMMA according to the programmed pattern.. (2) Following FIB exposure, the PMMA is developed and the exposed portions rinsed away. (3) The vanadium oxide is deposited by PLD in vacuum (with a few-nm thick overlayer of silver if needed to prevent charging), leaving behind (4) a layer of $VO_{1.7}$. (5) Following lift-off of the PMMA, the array is annealed in a low-pressure O_2 ambient, leaving behind an array of VO_2 nanodisks, or any other pattern programmed into the focused ion-beam pattern generator.

using a Lambda Physik CompEx 205 laser, at a pulse repetition frequency of 25 Hz. The fluence on the target was typically 4 mJ/cm^2, and typical deposition protocols required anywhere from 10,000 to 50,000 laser pulses. In the subsequent lift-off step, the remaining PMMA layer together with the $VO_{1.7}$ film deposited on it was removed by a commercial resist remover (Microposit 1165) leaving the $VO_{1.7}$ clusters resting on the ITO surface. Figure 3 shows schematically this lithography process, where regular arrays of 60 nm particles were obtained. The final stoichiometrically correct crystalline VO_2 is obtained by a 30 minutes of thermal annealing at 450 ºC in 250 mTorr of 0_2 background pressure. On insulating substrates where ion bombardment may charge the sample, a thin overlayer of silver may be deposited over the PMMA, as the Ga$^+$ ions will easily penetrate a conductive overlayer 10 nm or so thick.

A scanning electron microscope photograph of an array created by this process is shown in Figure 5. The nanoarticles are of order 75 nm in diameter and are spaced at intervals of 150 nm. The nanoparticles are not completely round, but their spacing is extremely regular. Nevertheless, the nanoparticles do exhibit optical switching, and RBS and XRD measurements show that the preponderance of material is in fact stoichiometrically correct VO_2.

Typical VO_2 patterns created by FIB lithography use a dose of 8×10^{-17} C per particle. Thus approximately 500 Ga$^+$ ions are required to expose a disk-shaped spot in the PMMA layer. Thus, even though the FIB typically has substantially less ion current than the electron beam in e-beam lithography, patterning times are similar, since for a given current the FIB requires 1/100 of the time used by the electron beam to complete the exposure of a particular spot. The actual resolution achieved in the patterning of the PMMA depends of course on the details of the spin-on coating process and the handling of the resist. It is likely that the above protocol, although dependable, is not by any means optimized. In particular, more sophisticated resists and advanced lift-off techniques should permit even higher-resolution array fabrication.

A number of different experiments were carried out in order to look for an optimum pulsed laser deposition and annealing protocol. In general, oxide films grown by UV-PLD are done by ablating the target into a background pressure of oxygen to make up for the oxygen typically lost during the deposition process. In fact, an important advantage of pulsed laser deposition technique resides in the fact that it can provide relatively easy stoichiometric control under high background gas pressure in thin oxide film deposition. The background vacuum level before introducing oxygen was kept under 3×10^{-6} Torr. The vanadium oxide deposition comprises two independent procedures. First, the thin vanadium oxide films were deposited on Si substrate at a room temperature with 5 mTorr oxygen gas. Rutherford backscattering (RBS) measurements showed these films to be in an intermediate oxidation state, close to amorphous $VO_{1.7}$. The thickness of the films was monitored by inserting a microscope slide next to the silicon
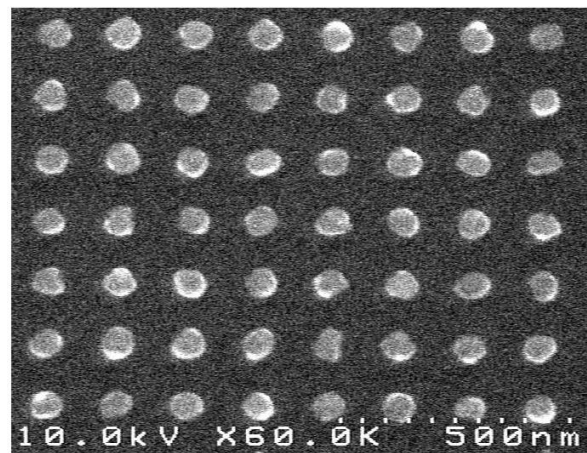

Figure 5. A nanodisk array produced by the combined FIB-PLD lithographic procedure.

surface as a witness sample; its thickness was then measured in a spectrophotometer to calibrate the thickness of the deposited vanadium oxide film.

Subsequently, the amorphous $VO_{1.7}$ films were annealed under an ambient of 250 mTorr oxygen at 450°C. X-ray diffraction measurements showed these films to be crystalline VO_2. The annealing temperature turned out to be critical: films annealed in the same oxygen ambient but at 550°C were V_2O_5; they exhibited no switching behavior and had characteristic V_2O_5 XRD spectra.
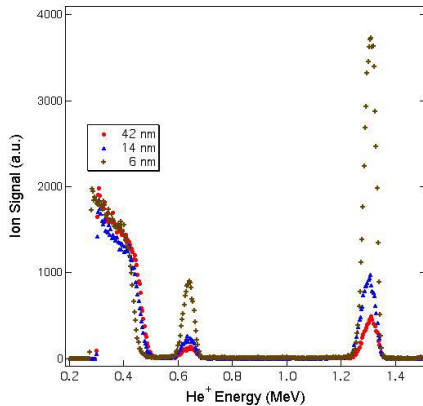
Figure 6. Rutherford backscattering spectra for films deposited at nominal thicknesses of 6, 14, and 42 nm. From left to right, the features in the spectra are the the oxygen background, the silicon peak and the vanadium peak.

Figure 7. Oxygen to vanadium ratio for films deposited by the PLD protocol outlined in the text and annealed at 450°C in 250 mTorr oxygen, as a function of deposited film thickness. Note the transition to the 2/1 stoichiometry at about 8 nm.

As is clear from Figure 3, vanadium oxides can exist in a wide range of stoichiometries, complicating the task of verifying that the nanoparticles created by this process are in fact VO_2. [18] Vanadium oxide films selectively deposited in the range of 10~250 mTorr oxygen pressure were investigated by Rutherford backscattering spectrum (RBS) in order to secure the correct 2:1 oxygen/vanadium ratio. None of the samples annealed at oxygen pressures below 250 mTorr oxygen gave the desired exact 2:1 ratio. However, at 450 °C under 250 mTorr O_2 pressure, $VO_{1.7}$ change rapidly into VO_2 without further conversion to higher phases. The RBS spectra of several vanadium oxide films deposited on graphite under the identical conditions are shown in Figure 6. In the given V/O ratio versus thickness graph (Figure 7), one can assure that the stoichiometry of the annealed films maintains a correct 1:2 ratio down to around 8 nm mass thickness. X-ray diffraction (XRD) scans obtained using a Scintag X_1 θ/2θ automated powder X-ray diffractometer with a Cu target and a Peltier-cooled solid-state detector (not shown here) confirmed the RBS results.
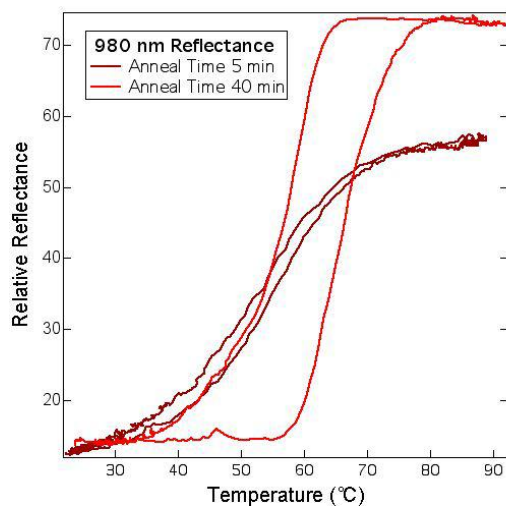
Figure 8. Scattered light intensity from a VO_2 nanoparticle film as a function of temperature, for two different annealing times. The change shows the evolution of stoichiometric vanadium dioxide.
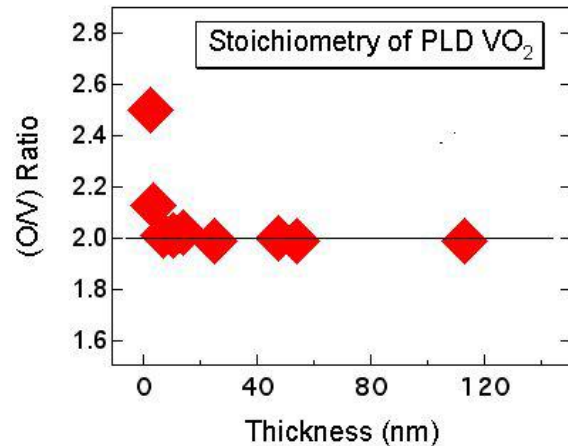
The transition temperature and hysteresis cycles of the 100 nm thick VO_2 films annealed at 450 °C were acquired by measuring the reflectance change to the infrared light at λ=980 nm during a heating and cooling. The transition temperature is taken as the midpoint on the heating curve. The films annealed for more than 20 minutes had a ~66 °C semiconductor-to-metal transition temperature, like the hysteresis curve in Figure 8. Apparently, the difference in the transition temperature comes from the enhancement in crystallinity as well as grain development and stress. [19] This is supported by the fact that those samples show better sharpness in the hysteresis loop and a relatively strong XRD intensity along the (011) plane. However, there is no further improvement in crystallinity for annealing times of 40 minutes or longer.

4. OPTICAL CHARACTERIZATION OF VO$_2$ NANODISK ARRAYS

Square two-dimensional arrays of single VO$_2$ nanodisks on silicon substrates, like those shown in Figure 5, were fabricated with lattice constants ranging from 147 to 397 nm. The optical properties of these nanostructures were measured by light scattering as shown schematically in Figure 9. The arrays were mounted on a heated stage and placed on a microscope platform. In this experimental arrangement, a confocal microscope is used to locate the array to be measured, which typically is a square pattern 50 to 100 μm on a side. The beam from the selected light source is focused into a ~200 μm spot which covers the array selected in the microscope. A thermoelectric heater can be used to alter the temperature of the array; the temperature was monitored by a thermocouple attached directly to the array. Photons radiated away by the particles are collected in a conventional confocal microscope or in an optical fiber. For incident white light, the scattered light was routed by a fiber optic cable into a spectrometer with a focal plane array detector. For measuring the hysteresis properties of the array, light from a near infrared laser (980 nm) was used for illumination, and the collected scattered light was carried by an optical fiber into a simple infrared detector.

Figure 9. Experimental geometry for measuring optical properties of VO$_2$ nanoparticle arrays. Scattered light from the arrays is focused by a lens onto an optical fiber connected to a spectrometer with focal plane array detector.

Regardless of the nature of the particles, whether in the metallic or semiconducting state, the geometrical arrangement obliges the particles to be a set of planar coherent scatterers. At points far away from the particles, the scattered electric field will be given by standard electromagnetic theory as [20]

$$\vec{E}(r\vec{s},\omega) \sim -k^2\{\vec{s}\times(\vec{s}\times\tilde{P}(r\vec{s},\omega))\}\frac{e^{ikr}}{r} \tag{1}$$

where $\vec{s}$ is the direction of observation, r is the distance from the position of the dipole source and k is the wavenumber. $\tilde{P}$ is the three dimensional Fourier transform of a constitutive relation approximated by $\tilde{P}(\vec{r}) = \alpha(\vec{r})\vec{E}^{(i)}(\vec{r})$, where $\alpha(\vec{r})$ represents the self-consistent polarizability [21] per unit volume of the scattering surface (which is only nonzero in the particles), and $\vec{E}^{(i)}(\vec{r}) = \hat{e}Exp(ik\vec{s}_o\cdot r)$ is the unperturbed field in the direction of the unit vector $\vec{s}_o$ with polarization $\hat{e}$. In this case of square lattices, $\tilde{P}$ is given by:

$$\tilde{P} = \alpha Nv\hat{e}\sum_{h,m} Sinc(h\pi a/L)\cdot Sinc(m\pi a/L)\cdot Sinc\left[\left(\frac{2\pi h}{L}+k(s_{ox}-s_x)\right)\frac{D}{2}\right]\cdot$$
$$Sinc\left[\left(\frac{2\pi m}{L}+k(s_{oy}-s_y)\right)\frac{D}{2}\right]\cdot Sinc\left[k(s_{oz}-s_z)\frac{b}{2}\right]Exp[ik\frac{b}{2}(s_{oz}-s_z)] \tag{2}$$

where *h* and *m* take all possible integer values. The particle is approximated as a parallelepiped of volume $v = a^2 b$. D is the side of the square array, L the lattice constant and N the total number of particles. Given that D is large compared with L and $v^{1/3}$, this scattering potential will have non-negligible values only when

$$s_x = s_{ox} + \frac{h\lambda}{L}, \qquad s_y = s_{oy} + \frac{m\lambda}{L} \qquad \text{with} \qquad s_x^2 + s_y^2 + s_z^2 = 1 \tag{3}$$

Clearly, the conditions expressed in equation (3) are completely equivalent to the diffraction from a two-dimensional grating. This diffractive effect is responsible for the colors observed in Figure 10, where the numerical aperture of the microscope objective limits the maximum angle allowed into the detection system and therefore the spectral spread in wavelengths admitted into the detector.

From the Poynting theorem and the content of equations (1) and (2), it is easy to see that in the scattered intensity, the optical material properties of the VO$_2$ nanoparticles as well as the influence of the surroundings are completely accounted for in the polarizability. Given the dual metal-semiconductor character of VO$_2$ the total optical response of the nanoparticles is expected to show profound differences when switching throughout the phase transition. The normal scattered intensity from monochromatic light of 980 nm wavelength and incident at 75º, shows a drop of 70% when
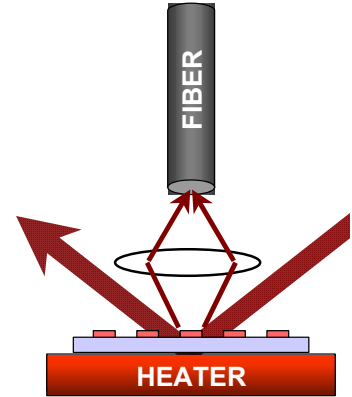
heated from the semiconducting to the metallic state. This is a very significant signal contrast given the short wavelength used in this measurement where the dielectric constants between the two VO_2 phases are very similar.   Comparable VO_2 particle densities, when measured in normal transmission mode with the same wavelength, showed less than 1% signal changes. The scattering measurement greatly enhances the signal contrast from small amounts of VO_2. On the other hand, the temperature measured with a precision thermocouple in contact with the sample, shows an onset of the phase transition similar to that found in standard VO_2 films. In the present case however, the VO_2 particles exhibit a large undercooling effect resulting in a hysteresis loop whose width spans ~ 35 ºC. This hysteresis width is significantly larger than values that are generally characteristic of bulk and thin film VO_2 samples; these normally have hysteresis of 1-10 ºC. [21]   Moreover, the enhanced hysteresis observed in the semiconductor-to-metal transition in small VO_2 nanocrystallites is definitely related to nanocrystallite size. [7]

Figure 10. Confocal microscope image of nc-VO_2 arrays ordered by increasing interparticle spacing from left to right.

A central unanswered questions about the structural semiconductor-to-metal (SMT) transition in vanadium dioxide is, how fast does it occur? Several groups have measured the transition in thin films using ultrafast laser and X-ray techniques; the phase transition in this case is initiated by a pump pulse that is strongly absorbed by the VO_2, creating dense electronic excitation. So far, there is agreement only that the transition occurs on a sub-picosecond time scale.

We have used femtosecond white-light continuum spectroscopy to see more clearly the temporal signature of the extremely broad surface plasmon resonance (SPR) at 1.1 µm. The probe beam, tightly focused into a thin silica plate, produces a continuous spectrum of light coherent with the pump beam; the pump beam excites the sample, generating the semiconductor-to-metal transition. The spectrum of the probe light, generated by focusing the light into an IR filter-glass plate, is approximately constant over the range 400-800 nm. Irradiation in the standard pump-probe arrangement produces a two-dimensional spectrum of sample transmission *vs* probe wavelength and pump-probe delay time. The advantage of displaying the data in this way is that one sees immediately the incipient plasmon response near 800 nm, whereas there is little change in the probe signal for wavelengths in the visible portion of the spectrum away from the SPR. The semiconductor-to-metal transition observed by this means occurs on a time scale of order 100 fs.
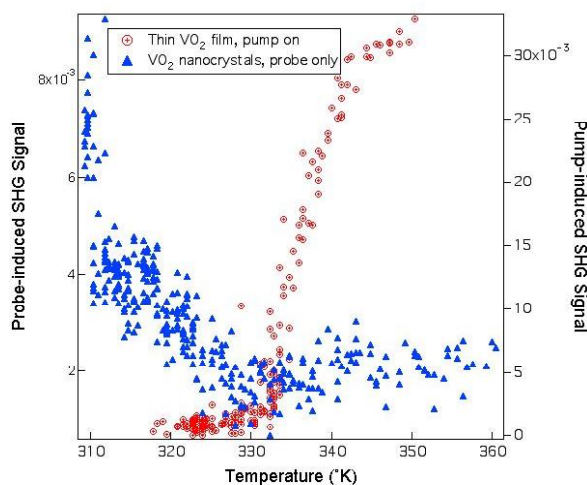
We have also tried a variant of pump-probe spectroscopy that involves observing the second harmonic of the probe beam. This produced a significant difference between the response of a vanadium dioxide thin-film sample and one containing VO_2 nanocrystals. In the experiment, a thin film or a nanocrystal composite of VO_2 on or in fused silica glass was heated above the metal-insulator transition temperature and then permitted to cool slowly while the pump-probe experiment was carried out with a 50 fs 800 nm laser. As seen in Figure 11, for the thin film, the probe-generated second-harmonic signal decreased as the transition to the semiconductor phase occurred; for the nanocrystalline material, on the other hand, the second-harmonic signal decreased. Since the second harmonic signal tends to be sensitive to surface effects, it is tempting to argue that this difference is due to the differing surface characteristics. The VO_2 film in the metallic state will be highly reflective, but the reflectivity will decrease as one moves to the semicon-

Figure 11.   Probe- and pump-induced second harmonic signals on vanadium dioxide nanoparticles and thin films, respectively.

ducting phase. However, the reason why the behavior in the nanocrystalline phase should be just the opposite remains obscure, something to be cleared up in future experiments.
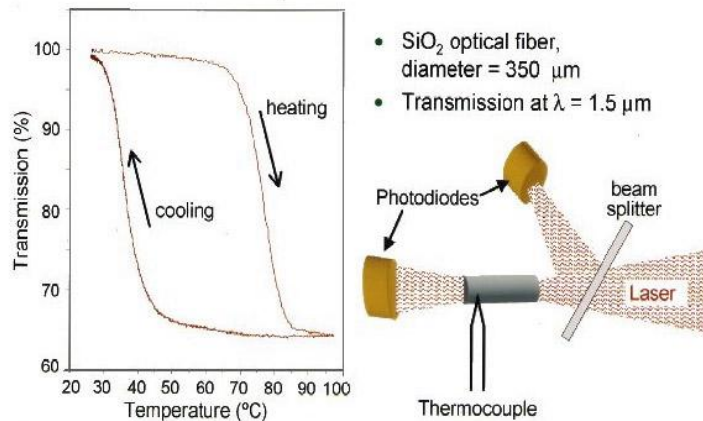
5. POTENTIAL APPLICATIONS AND PROSPECTS

- SiO$_2$ optical fiber, diameter = 350 μm
- Transmission at λ = 1.5 μm

Figure 12. (Left) Optical transmission of a fiber near the critical communications wavelength of 1.5 μm, showing the switching behavior as the embedded VO$_2$ nanocrystals were cycled between metallic and semiconducting states. The fiber was implanted with vanadium and oxygen ions to create a thin layer of VO$_2$ nanocrystals embedded in the leftmost end. From Reference [1].

Metal oxides as a class exhibit many interesting kinds of phase transitions, including superconductivity, magnetic ordering and other kinds of "smart" behavior. These variegated phenomena open the door to many potential applications. To show that a thin layer of VO$_2$ nanorods inside an optical fiber can exhibit switching or hysteretic behavior, in a geometry suitable for a sensor, vanadium and oxygen ions were implanted into one end of an optical fiber. Upon annealing, nanocrystals of VO$_2$ formed in a thin (100 nm) layer buried just under the surface of the fiber. A laser operating at 1.5 μm (the standard communications wavelength) was then focused through the fiber, as in Figure 12. A small heating element was attached to the end of the fiber, along with a thermocouple to measure the temperature, while optical detectors measured the light throughput.[22] The classic signature for smart behavior is the hysteresis loop shown in the left frame of the figure: As the temperature is raised, optical transmission remains high while the VO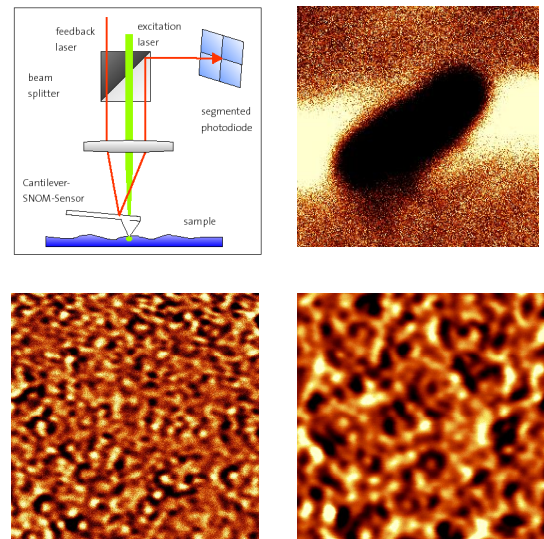$_2$ nanocrystals are in the semiconducting state. When the critical transition temperature is reached, the nanocrystals become metallic and the transmission drops abruptly as the layer of VO$_2$ nanocrystals reflects the incident light. As the optical fiber is cooled, the transmission remains low until a critical temperature near 40°C is reached, at which point the material becomes semiconducting again and transmits light as before. The hysteresis loop is even wider, and the switching behavior even more dramatic, in nanocrystals than in thin-film VO$_2$.

For the immediate future are studies of the semiconductor-to-metal transition in single VO$_2$ nanodisks are planned, using a scanning near-field optical microscope (SNOM). This is possibly the most important measurement that one could imagine on these nanoparticle arrays, since this would, in principle, permit the study of the semiconductor-to-metal transition in one nanoparticle at a time, as well as making environmental effects more controllable and reducing the effects on measurements of size inhomogeneity. We have recently begun attempts to image the VO$_2$ nanocrystals in a scanning near-field optical microscope as well as in a confocal microscope, and found that it is in fact possible to see individual nanoparticles. In Figure 13, the four quadrants show SNOM images of: (upper left) the geometry of the SNOM experiment; (upper right) a very large VO$_2$ nanoparticle, made by ion implantation and annealing, protruding through the surface of an alumina matrix; (lower left) an image of VO$_2$ nanoparticles, average size 37 nm radius, in a fused silica matrix, also made by ion implantation; and (lower right) an image of VO$_2$ nanoparticles, average size 73 nm, also made by ion implantation and annealing. The samples are not heated, so the nanoparticles are in the semiconducting state. This means that the nanoparticles are dark, since the visible light is absorbed (the semiconducting phase has a bandgap of order 1 eV), while the surrounding silica matrix is transparent to the green exciting beam.

Figure 13. Schematic of SNOM measurements, including (upper left) the geometry of the SNOM, and three measurements of VO$_2$ nanoparticles of varying sizes in alumina (upper right) and in fused silica (lower left and right). The picture dimension in all three cases is 6 μm.

6. SUMMARY AND CONCLUSIONS

The semiconductor-to-metal transition in vanadium dioxide has been an object of attention because of the scientific controversy over the mechanism of the transition, and the number of significant potential technological applications. The recent discovery that the optical effects caused by the metal-insulator transition are size dependent at the nanoscale has lent a sense of urgency to the need to synthesize VO_2 nanoparticles in regular arrays. This not only creates greater uniformity in the samples, but makes possible classes of measurements that have been impossible in samples synthesized in powders, gels or ion-implanted insulators. The work reported here demonstrates that a multi-step process involving focused ion-beam lithography, pulsed laser deposition, and post-deposition annealing can produce arrays with good size uniformity, uniform spacing, and interesting linear and nonlinear optical properties. In particular, the arrays show excellent hysteretic response over the temperature cycle that initiates and then relaxes the semiconductor-to-metal transition. Light-scattering measurements confirm the quality of the array fabrication by exhibiting diffraction-grating effects. Future work will emphasize scanning near-field microscopy of these arrays, with ultimate the goal of measuring the metal-insulator transition in single VO_2 nanoparticles.

7. ACKNOWLEDGEMENTS

REFERENCES

1. Capability for fabrication, testing of vanadium dioxide thin films developed to investigate potential for phase-transition devices. Journal of Research of the National Institute of Standards and Technology, 1997. 102(5): p. 597-597.

2. Morin, F.J., Oxides which Show a Metal-to-Insulator Transition at the Néel Temperature. Physical Review Letters, 1959. 3: p. 34-36.

3. Hanlon, T.J., et al., Comparison between vanadium dioxide coatings on glass produced by sputtering, alkoxide and aqueous sol-gel methods. Thin Solid Films, 2002. 405(1-2): p. 234-237.

4. Becker, M.F., et al., Femtosecond Laser Excitation of the Semiconductor-Metal Phase-Transition in VO_2. Applied Physics Letters, 1994. 65(12): p. 1507-1509.

5. Becker, M.F., et al., Femtosecond laser excitation dynamics of the semiconductor-metal phase transition in VO_2. Journal of Applied Physics, 1996. 79(5): p. 2404-2408.

6. Lopez, R., et al., Enhanced hysteresis in the semiconductor-to-metal phase transition of VO_2 precipitates formed in SiO_2 by ion implantation. Applied Physics Letters, 2001. 79(19): p. 3161-3163.

7. Lopez, R., et al., Size effects in the structural phase transition of VO_2 nanoparticles. Physical Review B, 2002. 65(22).

8. Srivasta.R and L.L. Chase, Raman Spectrum of Semiconducting and Metallic VO_2. Physical Review Letters, 1971. 27(11): p. 727-&.

9. Petrov, G.I., V.V. Yakovlev, and J. Squier, Raman microscopy analysis of phase transformation mechanisms in vanadium dioxide. Applied Physics Letters, 2002. 81(6): p. 1023-1025.

10. Pergament, A., Metal-insulator transition: the Mott criterion and coherence length. Journal of Physics-Condensed Matter, 2003. 15(19): p. 3217-3223.

11. Beteille, F. and J. Livage, Optical switching in VO_2 thin films. Journal of Sol-Gel Science and Technology, 1998. 13(1-3): p. 915-921.

12. Guzman, G., R. Morineau, and J. Livage, Synthesis of Vanadium Dioxide Thin-Films from Vanadium Alkoxides. Materials Research Bulletin, 1994. 29(5): p. 509-515.

13. Speck, K.R., et al., Vanadium Dioxide Films Grown from Vanadium Tetra-Isopropoxide by the Sol-Gel Process. Thin Solid Films, 1988. 165(1): p. 317-322.

14. Yi, X.J., et al., A new fabrication method for vanadium dioxide thin films deposited by ion beam sputtering. Infrared Physics & Technology, 2003. 44(2): p. 137-141.

15. Zheng, C.M., et al., Preparation of vanadium dioxide powders by thermolysis of a precursor at low temperature. Journal of Materials Science, 2000. 35(13): p. 3425-3429.

16. Gea, L.A. and L.A. Boatner, Optical switching of coherent VO_2 precipitates formed in sapphire by ion implantation and annealing. Applied Physics Letters, 1996. 68(22): p. 3081-3083.

17. Lopez, R., et al., Synthesis and characterization of size-controlled vanadium dioxide nanocrystals in a fused silica matrix. Journal of Applied Physics, 2002. 92(7): p. 4031-4036.

18. Nihoul, G., et al., Application of the static concentration waves theory to structural transitions in some oxides. Solid State Ionics, 1999. 117(1-2): p. 105-112.

19. Razavi, A., et al., Temperature Effects on Structure and Optical-Properties of Radio-Frequency Sputtered VO_2. Journal of Vacuum Science & Technology A-Vacuum Surfaces and Films, 1989. 7(3): p. 1310-1313.

20. Born, M. and E. Wolf, Principles of Optics. 7th ed. 2002, Cambridge UK: Cambridge University Press.

21. Jensen, T., et al., Electrodynamics of noble metal nanoparticles and nanoparticle clusters. Journal of Cluster Science, 1999. 10(2): p. 295-317.

22. Lopez, R., et al., Temperature-controlled surface plasmon resonance in VO_2 nanorods. Optics Letters, 2002. 27(15): p. 1327-1329.